

Ionic Liquid Filled Single-Walled Carbon Nanotubes for Flow-Induced Energy Harvesting

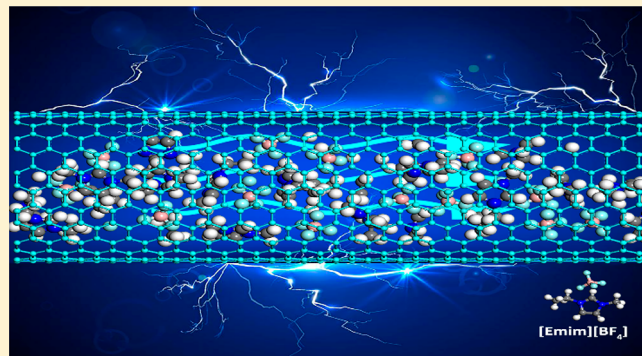
Yongji Guan,[†] Wenqiong Chen,[†] Jiao Zhang,[†] Fulong Yang,[†] Chao Du,[†] Xiaoping Zhang,^{*,†} and Youquan Deng^{*,†}

[†]Institute of Optoelectronics and Electromagnetic Information, School of Information Science and Engineering, Lanzhou University, Lanzhou, Gansu 730000, People's Republic of China

[‡]Centre for Green Chemistry and Catalysis, Lanzhou Institute of Chemical Physics, Chinese Academy of Sciences, Lanzhou, Gansu 730000, People's Republic of China

Supporting Information

ABSTRACT: Harvesting flow-induced energy for powering nanoelectromechanical systems offers much promise for nanotechnology. Motivated by the electric eel, which is capable of generating considerable electric shocks with highly selective ion channels and pumps on its cell membrane, herein, we employed molecular dynamics simulations to investigate the flow-induced energy harvesting through flowing three kinds of imidazolium-based ionic liquids (ILs) over single-walled carbon nanotubes (SWCNTs) with diameters varied from 1.22 to 4.07 nm at temperatures ranging from 300 to 375 K. The results show that ILs inside a SWCNT with a diameter of 3.39 nm flow at a speed of ~19 m/s resulting in a considerable flow-induced voltage (FIV) up to 2.22 μ V, and the maximal FIVs increase from 1.91 to 2.34 μ V as the diameter of the SWCNT varies from 1.22 to 4.07 nm at 300 K. Further analysis shows that this FIV arises from the free charge carriers on the inner surface of SWCNTs drifting along the flow direction of ILs under the drag of the Coulomb field, and the FIV increases to saturation with increased average flow velocity of ILs which is caused by the balance between internal resistance arising from the ILs and SWCNTs and the external driving force. This work also demonstrates an advanced equation to appropriately and effectively calculate the FIV of flowing ILs inside SWCNTs on the nanoscale which involves the effect of Coulomb field present in ILs on the free charge carriers of the SWCNT inner surfaces and the characteristic of Coulomb interactions. Moreover, the dependence of FIV on anion species, temperature, and average flow velocity of ILs is also investigated.



INTRODUCTION

With the rise of nanoscience and nanotechnology, harvesting clean energy directly from the ambient environment offers much promise for powering nanoelectromechanical systems.^{1–6} Since the electron drag of nanotube in flowing liquids was proposed in 2001,⁷ theoretical^{8–10} and experimental studies^{10–17} have illustrated that a flow-induced voltage (FIV) or electric current can be generated from flowing water and other polar liquids over carbon nanotubes (CNTs) along the flow direction. For experimental studies, flowing hydrochloric acid (HCl) solution over single-walled CNT (SWCNT) bulks filled between two metal electrodes with 1 mm spacing was reported to generate a FIV up to 10 mV along the flow direction. The generated FIV increases to saturation with increased average flow velocity (AFV) of the HCl solution, and the saturated value is significantly dependent on the polarity of the liquids and ionic conductivity but is about ten times smaller in multiwalled CNTs (MWCNTs).¹¹ In contrast, it was later reported that even flowing pure water over aligned MWCNTs films can generate a FIV up to 20 mV

and higher in flowing mild sodium chloride solutions.¹² Meanwhile, the research results also confirmed that the FIV also sensitively depends on the type of CNT, and flowing potassium chloride (KCl) solutions over the semiconducting SWCNTs film can generate a FIV three times higher than metallic SWCNTs film.¹⁸ For theoretical studies, although several different mechanisms, such as electron drag,⁷ streaming potential model,⁸ surface ions hopping (electronic friction against free electrons),¹⁹ pulsating asymmetric ratcheting,¹¹ and the mutual coupling of mobile dipoles and free charge carrier,^{13,14} have been proposed to elucidate the generation of the FIV in CNTs in the above-mentioned experiments, none of them can offer a satisfactory explanation for all observed phenomena.^{7–12,14,20}

However, the defects of the common liquids (methanol/ethanol aqueous solutions, KCl solutions, HCl solution, etc.)

Received: November 16, 2018

Revised: January 3, 2019

Published: January 4, 2019

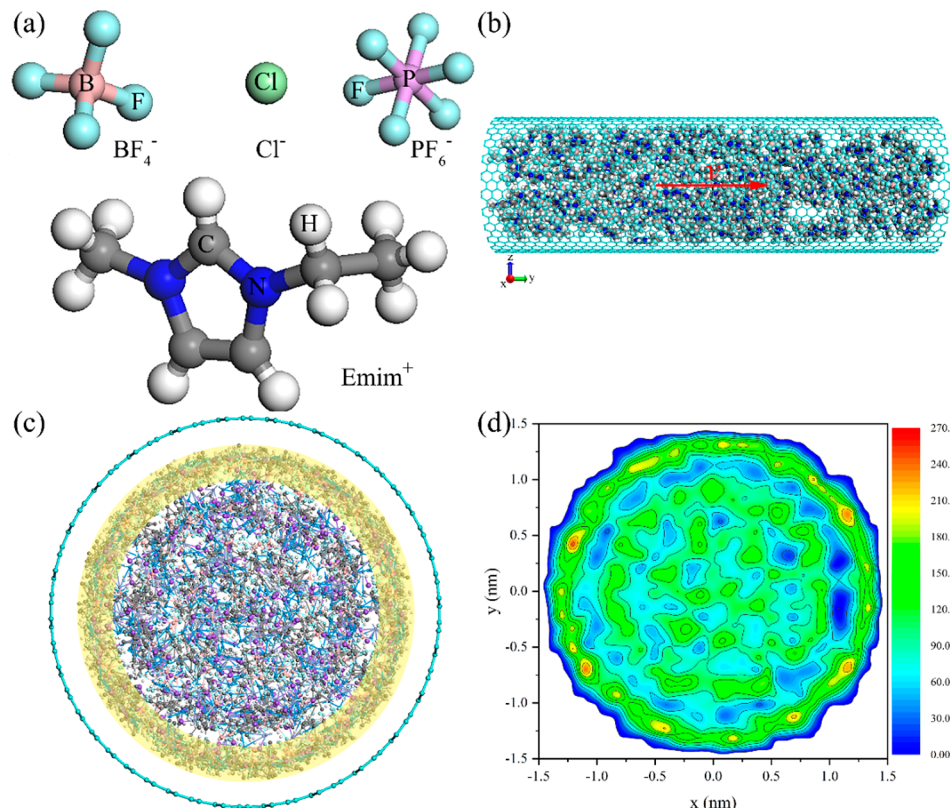


Figure 1. (a) The molecular structures of the ions constituting the ILs studied in this work, (b) an initial computational model of ILs [$\text{Emim}^+ \text{[BF}_4^-$] flowing inside a (25,25) SWCNT, (c) the radial equilibrium structure of the ILs [$\text{Emim}^+ \text{[BF}_4^-$] inside a (25,25) SWCNT at $T = 300\text{ K}$, and (d) contour plots of radial number density (atoms $\times \text{nm}^{-3}$) of the ILs [$\text{Emim}^+ \text{[BF}_4^-$].

applied in the above-mentioned experimental studies, such as being volatile, caustic, and virose, make it difficult to further apply the flow-induced energy harvesting system in health and related fields. Room temperature ionic liquids (ILs) are health-safe, environmentally friendly, and highly thermostable soft functional materials that can act as liquids in flow-induced energy harvesting systems,^{21–23} which can overcome the defects of common liquids and promote the further application of a flow-induced energy harvesting system. As reported in previous work, the ILs confined in SWCNTs exhibit an ultrafast diffusion due to low friction, molecular stacking, and cooperative dynamics effects, which benefits the FIV generation.²⁴ Moreover, the great technical complexity and experimental equipment make it difficult to observe the microscopic details of the nanoscale through experiments, while the molecular dynamics (MD) simulation is a powerful tool to understand molecular or atomic details and has been widely employed to various fields, such as the nanofluids, vibrational spectrum, and nanoconfined liquids.²²

Therefore, in this work, MD simulation is employed to probe the FIV generation by flowing three kinds of imidazolium-based ILs inside SWCNTs on the nanoscale. Flowing ILs inside SWCNT can generate a considerable FIV up to $2.22\text{ }\mu\text{V}$. We propose that this potential stems from the free charge carriers (FCCs) on the inner surfaces of SWCNTs drifting along the flow direction under the drag of the Coulomb field produced by ILs. Importantly, this work demonstrates an advanced equation, which can appropriately and effectively calculate the FIV of flowing ILs inside SWCNTs on the nanoscale taking the characteristic of Coulomb interactions and the effect of Coulomb field

produced by ILs on the FCCs of the SWCNT inner surfaces into consideration. In addition, this work also investigates the dependence of the FIV on anion species, temperature, and AFV, and the flow-induced energy harvesting system has great application potential in self-powered devices and systems.

■ MOLECULAR MODELS AND SIMULATION METHODS

In this work, MD simulation is employed to investigate the generation of the FIV through flowing ILs inside the SWCNTs under an acceleration. The molecular structures of three kinds of imidazolium-based ILs (1-ethyl-3-methylimidazolium chloride ([$\text{Emim}^+ \text{[Cl}^-$]), 1-ethyl-3-methylimidazolium tetrafluoroborate ([$\text{Emim}^+ \text{[BF}_4^-$]), and 1-ethyl-3-methylimidazolium hexafluorophosphate ([$\text{Emim}^+ \text{[PF}_6^-$])) simulated in this work and an initial ensemble structure consisting of the cylindrical bulk ILs and a SWCNT are presented in Figure 1a,b, respectively. The main reason for choosing these three kinds of ILs is that they have the same cations, while the anions have a symmetrical structure (a center of inversion or tetrahedral symmetry). As shown in Figure 1b, the initially cylindrical structures are stochastically comprised of some ion pairs of ILs using the PACKMOL software.²⁵ The SWCNTs are selected from a segment of (9,9), (12,12), (16,16), (20,20), (25,25), and (30,30) CNTs with diameter of 1.220, 1.627, 2.170, 2.712, 3.390, and 4.068 nm and length of 10.944 nm. For the MD simulation presented in this work, the number of ion pairs is calculated taking the effective diameter of the SWCNT into consideration. The effective diameter of the SWCNT for occupancy of cations and anions is estimated as $D_{\text{eff}} = D_{\text{CNT}} - 2\sigma_c$, where σ_c is the van der Waals (vdW) radius of carbon

(0.17 nm). The ion pairs of ILs inside different SWCNTs are presented in Table 1. The SWCNTs are flexible, but their

Table 1. Ion Pairs of Three Kinds of ILs for Different SWCNTs

	(9,9)	(12,12)	(16,16)	(20,20)	(25,25)	(30,30)
[Emim][BF ₄]	26	55	111	186	308	460
[Emim][PF ₆]	22	47	96	161	266	397
[Emim][Cl]	30	65	131	220	363	543

centers of mass are fixed to prevent the SWCNTs from shifting in the simulation. The size of the simulation box is set as $11.0 \times 11.0 \times 11.0$ nm³ to avoid interactions with neighbor cells (x and z directions). The ensemble structure is the center of the simulation box.

The MD simulation package DL_POLY 4.08 is employed to all MD simulations in this work.²⁶ An all-atom force field developed by Wang and co-workers is used for intra- and intermolecular interactions.²⁷ The vdW parameters for unlike atoms are mixed by the Lorentz–Berthelot combining rule.²⁸ The 12-6 Lennard–Jones potential parameters of carbon atoms in SWCNTs are 0.4056 kJ·mol⁻¹ and 0.34 nm.¹⁹ The velocity verlet algorithm is used to integrate the Newton's motion equation. The Nosé–Hoover thermostat^{29,30} with a relaxation time constant of 1.0 ps is employed to maintain a desired system temperature (varying from 300 to 375 K). The distance of the Lennard–Jones and electrostatic interactions is cut off in 1.5 nm. The smooth particle mesh Ewald method is used to deal with the long-range Coulomb interaction.³¹ Periodic boundary conditions are applied to all directions of the simulated box.

The simulated ILs are equilibrated by a simulated annealing procedure as follows. The initial random configuration goes through a series of NPT simulations at a constant pressure $P = 100$ atm and different temperatures from $T = 1000$ K down to 800, 600, 400, and 300 K. At each temperature, the system is simulated for 1 ns. The last configuration was then equilibrated with a 5 ns NPT simulation at $P = 1$ atm and $T = 300$ K to obtain the average simulation volume V . After that, the ILs further go through another simulated annealing procedure in the NVT ensemble with the same temperature sequence and the determined V . After 20 ns of NVT simulation, the total energy of the simulated system slightly fluctuates around a fixed value (Figure S1) and the system reaches equilibration. The obtained ILs equilibrium configuration and SWCNT are then allowed to run for 20 ns to ensure a better equilibrium state under the NVT ensemble at $T = 300$ K. Then, a series of accelerations (from 0.001 to 0.2 nm·ps⁻²) are applied only in the axial direction of the SWCNT for another 20 ns simulation to make the simulation system reach a better equilibration state. When the ILs show a steady flow in the SWCNT, the corresponding statistical average data are collected and analyzed. For the simulation systems at other temperatures ($T = 325$, 350, and 375 K), similar procedures are adopted. Thus, this can ensure the reliability of the results. The DL_POLY analysis package³² and the visual molecular dynamics (VMD) software³³ are used to characterize the physical properties and visualize the structures of simulated systems, respectively.

RESULTS AND DISCUSSION

Number Density Distribution. After the simulated systems reach the equilibration, the ions distribution inside the SWCNT is first investigated because it directly determines the FIV generation. Taking the [Emim][BF₄] ILs inside a (25,25) SWCNT as a representative example, the equilibrated system structure is shown in Figure 1c. As can be seen from Figure 1c, more anions and cations aggregate on the inner surface of SWCNT to form the stronger adsorbed layers (the shaded region in Figure 1c) that are generally called the first solvation shell (FSS); this is confirmed by the radial number density of the [Emim][BF₄] ILs presented in Figure 1d. Figure 1d indicates the radial number density of ions exhibits larger fluctuations and reaches maximal values near the inner surface of SWCNT. The radial number density of ions near the inner surface of SWCNT almost doubles compared to the bulk number density in central region of SWCNT which could be attributed to the vdW interactions between ILs and SWCNT. Meanwhile, we also calculate the axial number density of cations and anions and find it fluctuates across a constant value and the distinct layers do not occur in the axial direction (Figure S2b). Therefore, only the influence of ions distribution in the radial direction is involved in calculating the FIV in this work, and the axial distribution of cations and anions is not considered.

Calculated Equation for Flow-Induced Voltage. In this work, the charged cations and anions naturally and inevitably lead to Coulomb field presented around them. When the cations and anions move inside a (25,25) SWCNT at a constant velocity, the fluctuating Coulomb field presented around the ILs drags the FCCs on the SWCNT's surface to drift in the direction of ILs flow. Thus, this generates a FIV due to FCCs drifting along the SWCNT surfaces. Under these circumstances, the previous reported equation¹⁶ only taking the effect of the anions in the generation of FIV into consideration is not appropriate for calculating this FIV of flowing ILs in a SWCNT because the FCCs on the inner surface of the SWCNT drift along the flow direction under the drag of the Coulomb field produced by cations and anions in the FSS together and they all devote to the generation of the FIV. It is worth noting that the driving anions could generate a current in the opposite flow direction, which could counteract or reduce the current generated by driving cations along the flow direction. Thus, the FIV of flowing ILs in a SWCNT could be estimated considering the effect of cations as

$$V = R\sigma eL(v^+ - kv^-) \quad (1)$$

where the resistance R is dependent on the CNT structure as $R = 4R_0L/(\pi D^2)$, R_0 is the reference resistance of 400 Ω·nm, and D is the diameter of the SWCNT.³⁴ σ represents the average FCCs density of the SWCNT and is about 0.89×10^{20} m⁻²; e is the electronic charge (1.6×10^{-19} C). L is the length of the SWCNT. v^+ and v^- are the AFVs of cations and anions, respectively. k is a correction term introduced by the converse contribution of anions to the generation of FIV.

On the other hand, flowing ILs inside the SWCNT can make cations and anions accumulate on the inner surface of the SWCNT to form the FSS (Figure 1c) due to the vdW interactions between SWCNT and ILs. The radial number density of ions in the FSS almost doubles compared to the bulk number density in the central region of the SWCNT, and this makes the radial charge densities of cations and anions ($\rho^+(r)$

and $\rho^-(r)$) exhibit larger and different values (Figure 2). Thus, the correction term k in eq 1 could be expressed as

$$k = \frac{\rho^-(r)}{\rho^+(r)} \quad (2)$$

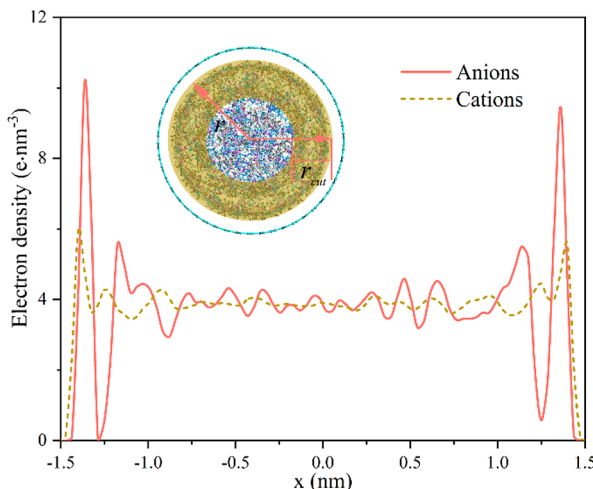


Figure 2. Radial charge density of ions at $T = 300$ K, where the inset shows the range (r_{cut}) of Coulomb field effect on FCCs.

Furthermore, Coulomb interaction strengths between ILs and the FCCs on the inner surface of the SWCNT are directly proportional to the charge and inversely proportional to the square of the distance. Considering this characteristic of Coulomb interactions, the radial charge densities of anions and cations can be modified as $\frac{1}{r^2}\rho^-(r)$ and $\frac{1}{r^2}\rho^+(r)$. Nevertheless, since the factor $\frac{1}{r}$ has been considered in calculating radial charge densities of cations and anions, the modified radial charge densities for anions and cations should be expressed as $\frac{1}{r}\rho^-(r)$ and $\frac{1}{r}\rho^+(r)$. Last but not least, all the effect of the Coulomb field generated by cations and anions in the FSS and bulk on the FCCs should be considered. That is, the modified radial charge densities should be integrated in the range of Coulomb field effect on FCCs (from r_0 to r , $r = r_0 + r_{\text{cut}}$). Therefore, eq 2 could be further expressed as

$$k = \frac{\left| \int_{r_0}^r \frac{1}{r} \rho^-(r) dr \right|}{\left| \int_{r_0}^r \frac{1}{r} \rho^+(r) dr \right|} \quad (3)$$

Replacing k in eq 1 using eq 3, we obtain the compact expression to calculate the FIVs of flowing ILs inside a SWCNT as

$$V = R\sigma e L \left(v^+ - \frac{\left| \int_{r_0}^r \frac{1}{r} \rho^-(r) dr \right| v^-}{\left| \int_{r_0}^r \frac{1}{r} \rho^+(r) dr \right|} \right) \quad (4)$$

Flow-Induced Voltage Generation. To drive the ILs flowing along the SWCNT, an acceleration is exerted on the ILs in the axial direction. Under an acceleration, the cations and anions of ILs are driven to move along the axial direction of the SWCNT. According to the simulated results, the accumulated displacements of cations and anions inside a

(25,25) SWCNT under an applied acceleration of $0.15 \text{ nm}\cdot\text{ps}^{-2}$ in axial and radial direction are calculated and the axial accumulated displacements are much larger than that in the radial direction. This means that an external driving force (EDF) is applied in the axial direction and drives the cations and anions to move inside a (25,25) SWCNT along the axial direction. The accumulated displacements of cations and anions in the axial direction are calculated and shown in Figure 3. It can be clearly seen from Figure 3 that the growth rate of

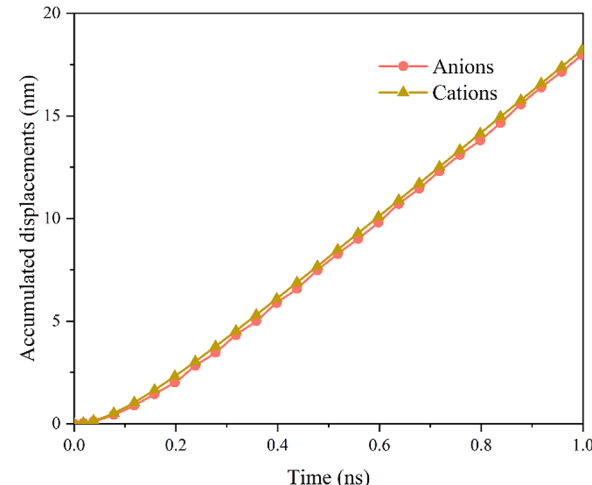


Figure 3. Accumulated displacements of ions inside a (25,25) SWCNT under a $0.15 \text{ nm}\cdot\text{ps}^{-2}$ acceleration at $T = 300$ K.

accumulated displacements of cations and anions gradually increases to a constant over time; that is, the slope of the accumulated displacements curves of cations and anions increases with time and then tends to a fixed value. These results indicate that the AFVs of cations and anions nonlinearly increase and then tend to saturation over time, which provides an analogous result with previous study.^{16,35} Meanwhile, Figure 3 also indicates that the accumulated displacements of cations are slightly greater than the anions. The larger accumulated displacements of cations could be caused by the different viscous drag produced by internal ILs and friction generated by SWCNT for cations and anions. Due to a flatter structure of the cation than the anion, the cation receives less viscous drag compared to the anion. On the other hand, the symmetry of the cation may allow for its faster movement in the imidazolium ring plane (axial direction) than in the normal to the imidazolium ring direction (radial direction).³⁶ To further understand the difference of accumulated displacements between cations and anions, we calculate the mean square displacements (MSDs) of cations and anions inside a (25,25) SWCNT and find the MSDs of cations are slightly greater than anions; the results are presented in Figure S3.

On the basis of the accumulated displacements in the axial direction, the AFVs of cations and anions in flow direction at different accelerations are calculated and presented in Figure 4. It is shown that the AFVs of cations and anions nonlinearly increase in the initial stage under an applied acceleration and then gradually tend to be saturated over time. Generally speaking, the velocity of the object is proportional to the acceleration it receives and will continually increase under an acceleration over time. However, the AFVs of cations and anions shown in Figure 4 exhibit a saturation rather than a continuous linear increase. In fact, when the cations and anions

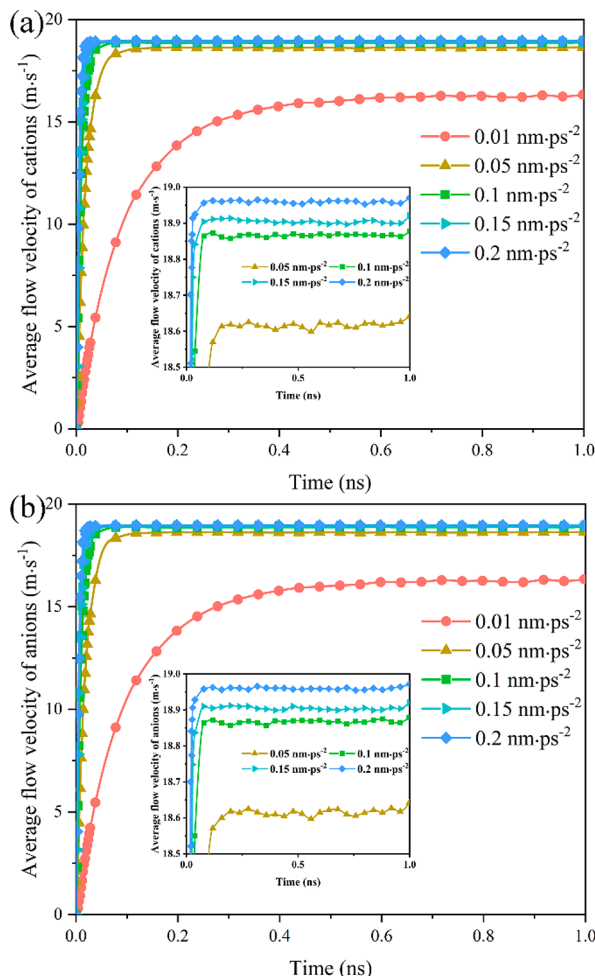


Figure 4. AFV of cations and anions in (a) and (b), changing with simulated time under different accelerations at $T = 300\text{ K}$.

move inside a SWCNT, the cations and anions are subject to EDF arising from applied acceleration, the viscous drag generated by internal ILs, and friction produced by SWCNT. The balance between viscous drag, friction, and EDF leads to this saturation phenomenon. As a universal principle, viscous drag is proportional to the velocity at which an object moves in a liquid. Under an acceleration, the AFVs of cations and anions increase over time, and meanwhile, the viscous drag also increases. When the sum of viscous drag and friction is equivalent to the EDF, the AFVs of cations and anions do not further increase and thus show a saturation trend. Figure 4 also demonstrates that the ultrasaturated AFVs of cations and anions increase as the applied acceleration increases. A larger acceleration means that a larger EDF is imposed on the cations and anions, and to overcome this larger EDF, a larger viscous drag is needed. Consequentially, the AFVs of cations and anions will increase and produce a larger viscous drag to balance a larger EDF.

On the basis of the above-mentioned advanced eq 4, the FIV for the ILs [Emim][BF₄] flowing inside a (25,25) SWCNT is calculated and the result is presented in Figure 5. As is clear from Figure 5, the relatively small size model of ILs [Emim][BF₄] flowing in a (25, 25) SWCNT produces a FIV of about 2.22 μV at $T = 300\text{ K}$. This value is slightly less than the FIV (2.32 μV) produced by a nanoscale ILs [Emim][BF₄] droplet flowing over a single-layered graphene,³⁵ and the small

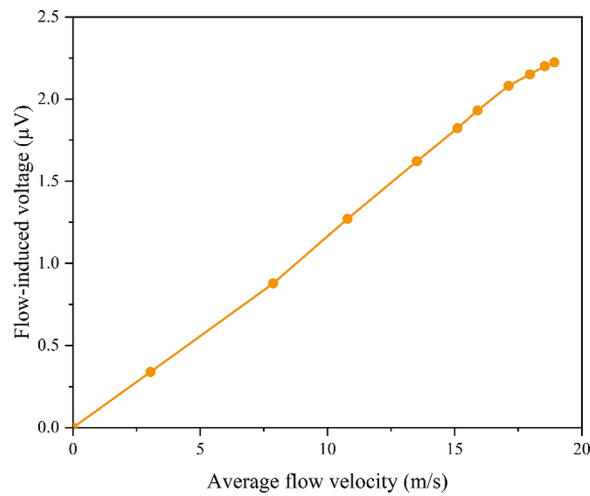


Figure 5. FIV as a function of varying AFV under a $0.15\text{ nm}\cdot\text{ps}^{-2}$ acceleration at $T = 300\text{ K}$.

difference could be caused by the extra larger viscous drag and friction from the SWCNT applied to the ILs. Meanwhile, Figure 5 also demonstrates that the FIV exhibits an approximately linear increase and then tends to saturation as the AFV increases, which is qualitatively similar to previous experimental and computational results^{10,11,16,35,37} and arises from the balance between viscous drag from internal ILs, friction from SWCNT, and EDF from an applied acceleration. When cations and anions move along the axial direction of SWCNT under an applied acceleration, the cations and anions also hop in the radial direction of SWCNT. This leads to a smaller radial displacement of cations and anions; thus, the flow-induced voltage exhibits an approximately linear increase.

Diameter of SWCNT Effect. It is well-known that the diameter of the SWCNT significantly affects the extent of nanoconfinement, thus affecting the AFVs of cations and anions. Employing different diameters, such as 1.220, 1.627, 2.170, 2.712, 3.390, and 4.068 nm, would allow for interference of the effect of the SWCNT diameter on the FIV. The equilibrated structures of ILs [Emim][BF₄] inside SWCNTs of different diameters at $T = 300\text{ K}$ are presented in Figure S4, and the average number and charge density in the radial direction are shown in Figure S5. Under a $0.15\text{ nm}\cdot\text{ps}^{-2}$ acceleration, the cations and anions inside different SWCNTs obtained different AFVs and the AFVs of cations and anions increase as the diameter of the SWCNT increases (Figure S6). A larger diameter of the SWCNT may result in the larger numbers of ions, which are away from the inner surface of the SWCNT, and the smaller numbers of collisions per unit volume to increase the AFVs.^{22,37,38} Meanwhile, the interactions between the SWCNT and ions decrease as the diameter of the SWCNT increases, and thus, cations and anions obtain the larger AFVs. The tendency can be quantified by the radial distribution function (RDF) arising from the MD simulation results presented in Figure S7, and the peak values of the RDFs decrease as the diameter of the SWCNT increases. This weakens the interaction between SWCNT and ILs and the friction from the SWCNT toward the cations and anions and increases the AFVs of cations and anions. However, as the diameter of the SWCNT increases, the AFVs do not continue to increase because the viscous drag caused by the internal ILs plays a significant role in the larger diameter SWCNTs and imposes restriction on the increase in the AFVs.

When the viscous drag caused by the internal ILs and the friction generated by the SWCNT are equal to the EDF produced by the applied acceleration, the AFVs do not further increase and then exhibit a saturation trend. Since the AFVs of cations and anions increase as the diameter of the SWCNT increases, according to the advanced eq 4 we developed, the FIVs also increase as the diameter of the SWCNT increases and then tend to saturation, as shown in Figure 6.

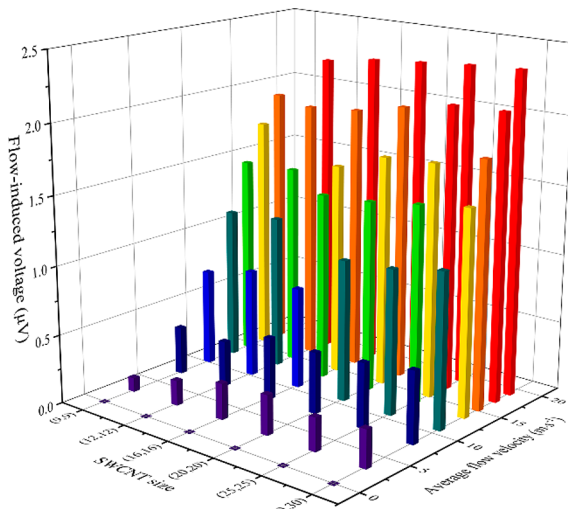


Figure 6. FIV as a function of the AFV for different SWCNTs under a $0.15 \text{ nm}\cdot\text{ps}^{-2}$ acceleration and $T = 300 \text{ K}$.

Anion Species Effect. The anion species largely determine the transport properties of ILs^{39,40} and thus affect the AFVs of cations and anions. In this work, three kinds of imidazolium-based ILs including different anions (BF_4^- , PF_6^- , and Cl^-) filled inside (25,25) SWCNTs are carried out to anatomize the influence of anion species on the FIV generation. The same temperature ($T = 375 \text{ K}$) is employed for all ILs to ensure the reliability of the simulation results. For three equilibrated systems, more cations and anions aggregate on the inner surface of SWCNTs to form the FSS due to the strong interaction between ILs and SWCNTs; the radial number density of ions exhibits larger fluctuations and reaches maximal values near the inner surface of SWCNTs which almost doubles compared to the bulk phase. Considering the distribution of cations and anions of three kinds of ILs, we calculate the AFVs of cations and anions for three kinds of ILs inside (25,25) SWCNTs and the results are presented in Figure S8. By comparing the calculated AFVs of cations and anions for three kinds of ILs inside (25,25) SWCNTs, we find that the AFVs of anions follow the order $\text{Cl}^- > \text{BF}_4^- > \text{PF}_6^-$ (Figure S8b). Since these three kinds of ILs have the same cation and the anions have a center of inversion or tetrahedral symmetry, according to previously reported results,^{38,39,41} the diffusion of these three kinds of ILs is mainly dependent on the volume of anion. Obviously, the volumes of anions follow the order $\text{Cl}^- < \text{BF}_4^- < \text{PF}_6^-$.⁴² As the anion volume increases, the viscous drag arising from surrounding anions and cations also increases. Thus, the transfer ability of the anion decreases, and the AFV of anion decreases. Due to the stronger interaction between cation and anion, the transfer ability of the corresponding cation decreases and the AFV of the cation also decreases. That is, the AFVs of cations also follow the

order $[\text{Emim}][\text{Cl}] > [\text{Emim}][\text{BF}_4] > [\text{Emim}][\text{PF}_6]$ (Figure S8a). On the basis of the AFVs of cations and anions and our developed advanced eq 4, the FIVs are calculated and presented in Figure 7. The effect of microstructural changes

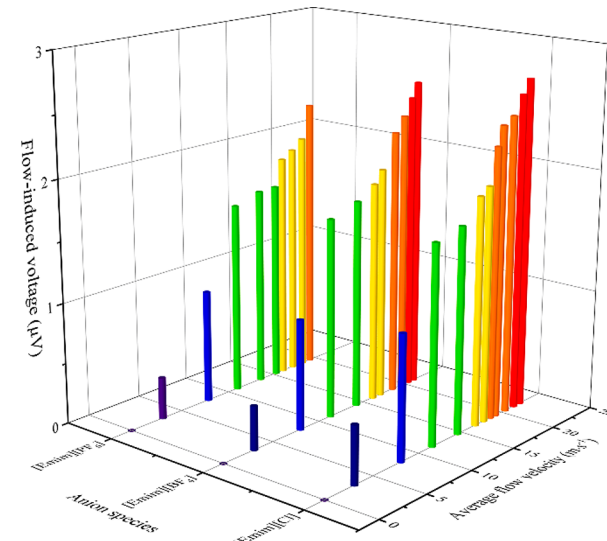


Figure 7. FIV as a function of the AFV for different anion species under a $0.15 \text{ nm}\cdot\text{ps}^{-2}$ acceleration and $T = 375 \text{ K}$.

of these three kinds of ILs inside (25,25) SWCNTs on the FIVs is considered in calculating the radial charge density of cations and anions in eq 4. From Figure 7, we can find that the FIVs of different ILs inside a (25,25) SWCNT also increase to saturation as the AFVs increase.

System Temperature Effect. Due to the high sensitivity of physicochemical properties of nanoconfined ILs toward temperature,²² probing the dependence of the FIV on temperature is a significant point. Therefore, the dependence of the FIV on temperature is probed at $T = 300, 325, 350$, and 375 K in this work. Following a similar procedure, the AFVs of cations and anions are calculated in accordance with the accumulated displacements and the results are presented in Figure S9. As the temperature increases, the increased distance between cations and anions makes the binding effect of Coulomb interactions in ILs on cations and anions be weakened and the ions obtain good mobilities. Thus, the cations and anions drift at larger AFVs inside a (25,25) SWCNT. The mobilities of cations and anions can be confirmed by the MSDs^{21,28,37} of themselves originated from the simulated results. Figure S10 shows the calculated MSDs of ions, and it visually shows that the MSDs of ions exhibit an increase as the temperature increases from 300 to 375 K . This increase manifests that the ions can more easily exit from their start positions to get larger velocities, which is confirmed by the AFVs plotted in Figure S9. Similarly, the FIVs are calculated according to the AFVs of cations and anions from 300 to 375 K , and the results are presented in Figure 8. Obviously, the AFVs increase as the temperature increases from 300 to 375 K , and a $2.60 \mu\text{V}$ peak FIV generates from flowing ILs inside a (25,25) SWCNT at $T = 375 \text{ K}$ which has a 16% increase compared to the value at $T = 300 \text{ K}$. It is worth noting that a similar saturation trend also exists as the AFVs increase to saturation; this could be attributed to the viscous drag generated by inner ILs and friction arising from SWCNT.

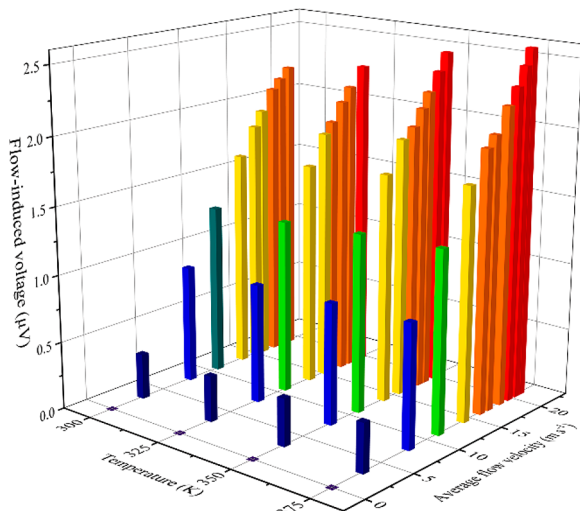


Figure 8. FIV as a function of varying AFV under a $0.15 \text{ nm}\cdot\text{ps}^{-2}$ acceleration at $T = 300, 325, 350$, and 375 K .

CONCLUSION

In summary, the generation of FIV is probed through flowing three kinds of imidazolium-based ILs inside SWCNTs using MD simulations on the nanoscale. The simulated results show that flowing ILs [Emim][BF₄] inside a (25,25) SWCNT at a speed of $\sim 19 \text{ m/s}$ can generate a considerable FIV up to $2.22 \mu\text{V}$ at $T = 300 \text{ K}$. This potential arises from the FCCs on the inner surfaces of SWCNTs drifting along the flow direction under the drag of the Coulomb field produced by ILs. The FIV increases to saturation as the AFV increases which is caused by the balance among the EDF coming from applied acceleration, internal viscous drag generated by inner ILs, and friction produced by SWCNT. Significantly, an advanced equation is modified to appropriately and effectively calculate the FIV of flowing ILs inside SWCNTs on the nanoscale involving the effect of Coulomb field produced by ILs on the FCCs of the SWCNT inner surfaces and the characteristic of Coulomb interactions. Analyzing the simulated results confirms that the FIVs increase from 1.91 to $2.34 \mu\text{V}$ as the diameters of SWCNTs vary from 1.22 to 4.07 nm at $T = 300 \text{ K}$, and meanwhile, the FIV also increases as the volume of anion decreases ($\text{PF}_6^- > \text{BF}_4^- > \text{Cl}^-$). Additionally, the simulated results also indicate that the FIV increases as AFV and temperature increase which is caused by the cooperative effect among the EDF arising from applied acceleration, the viscous drag generated by internal ILs, and friction produced by SWCNT, and a $2.60 \mu\text{V}$ peak FIV generates from flowing ILs inside a (25,25) SWCNT at $T = 375 \text{ K}$ which has a 16% increase compared to the value at $T = 300 \text{ K}$. We hope this work will greatly enhance understanding of the FIV on the nanoscale and accelerate the process of the flow-induced energy harvesting in self-powered devices and systems.

ASSOCIATED CONTENT

Supporting Information

The Supporting Information is available free of charge on the ACS Publications website at DOI: [10.1021/acs.jpcc.8b11142](https://doi.org/10.1021/acs.jpcc.8b11142).

Variation of total energy of the simulation system consisting of [Emim][BF₄] and SWCNT with relaxation time steps, the axial equilibrium structure of the ILs [Emim][BF₄] inside a (25,25) SWCNT, the mean

number density of cations and anions in axial direction inside a (25,25) SWCNT at $T = 300 \text{ K}$, MSDs of cations and anions for ILs [Emim][BF₄] inside a (25,25) SWCNT at $T = 300 \text{ K}$, the equilibrated structures of ILs [Emim][BF₄] inside SWCNT of different diameters at $T = 300 \text{ K}$, the radial number and charge density of cations and anions inside SWCNT of different sizes, average flow velocity of cations and anions varying with time under different pore size at $T = 300 \text{ K}$, center of mass RDFs for cations and anions around the carbon atoms of SWCNTs, average flow velocity of cations and anions for three kinds of ILs inside a (25,25) SWCNT at $T = 375 \text{ K}$, average flow velocity of cations and anions for ILs [Emim][BF₄] inside a (25,25) SWCNT at $T = 300, 325, 350$, and 375 K , and MSDs of cations and anions for ILs [Emim][BF₄] inside (25,25) SWCNT at $T = 300, 325, 350$, and 375 K ([PDF](#))

AUTHOR INFORMATION

Corresponding Authors

*E-mail: zxp@lzu.edu.cn.

*E-mail: ydeng@licp.acs.cn.

ORCID

Yongji Guan: [0000-0001-9210-3530](https://orcid.org/0000-0001-9210-3530)

Xiaoping Zhang: [0000-0003-0046-211X](https://orcid.org/0000-0003-0046-211X)

Youquan Deng: [0000-0002-7612-0354](https://orcid.org/0000-0002-7612-0354)

Notes

The authors declare no competing financial interest.

ACKNOWLEDGMENTS

The authors acknowledge the financial support of this work from the National Key Research and Development Program of China (2017YFA0403101), the Fundamental Research Funds for the Central Universities (No. lzujbky-2018-it62 and No. lzujbky-2018-127), the Double first class Funding-International Cooperation and Exchange Program (227000-560001), the National Natural Science Foundation of China (61804071), and the Natural Science Foundation of Gansu Province (17JR5RA119).

REFERENCES

- Park, J.; Song, S.; Shin, C.; Yang, Y.; Weber, S. A. L.; Sim, E.; Kim, Y. S. Ion Specificity on Electric Energy Generated by Flowing Water Droplets. *Angew. Chem., Int. Ed.* **2018**, *57*, 2091–2095.
- Cottrill, A. L.; Liu, A. T.; Kunai, Y.; Koman, V. B.; Kaplan, A.; Mahajan, S. G.; Liu, P.; Toland, A. R.; Strano, M. S. Ultra-High Thermal Effusivity Materials for Resonant Ambient Thermal Energy Harvesting. *Nat. Commun.* **2018**, *9*, 664.
- Kim, S. H.; Haines, C. S.; Li, N.; Kim, K. J.; Mun, T. J.; Choi, C.; Di, J.; Oh, Y. J.; Oviedo, J. P.; Bykova, J.; et al. Harvesting Electrical Energy from Carbon Nanotube Yarn Twist. *Science* **2017**, *357*, 773.
- Zhong, H.; Xia, J.; Wang, F.; Chen, H.; Wu, H.; Lin, S. Graphene-Piezoelectric Material Heterostructure for Harvesting Energy from Water Flow. *Adv. Funct. Mater.* **2017**, *27*, 1604226.
- Yin, J.; Li, X.; Yu, J.; Zhang, Z.; Zhou, J.; Guo, W. Generating Electricity by Moving a Droplet of Ionic Liquid Along Graphene. *Nat. Nanotechnol.* **2014**, *9*, 378.
- Xu, S.; Qin, Y.; Xu, C.; Wei, Y.; Yang, R.; Wang, Z. L. Self-Powered Nanowire Devices. *Nat. Nanotechnol.* **2010**, *5*, 366.
- Král, P.; Shapiro, M. Nanotube Electron Drag in Flowing Liquids. *Phys. Rev. Lett.* **2001**, *86*, 131–134.
- Cohen, A. E. Carbon Nanotubes Provide a Charge. *Science* **2003**, *300*, 1235.

- (9) Persson, B. N. J.; Tartaglino, U.; Tosatti, E.; Ueba, H. Electronic Friction and Liquid-Flow-Induced Voltage in Nanotubes. *Phys. Rev. B: Condens. Matter Mater. Phys.* **2004**, *69*, 235410.
- (10) Ghosh, S.; Sood, A. K.; Ramaswamy, S.; Kumar, N. Flow-Induced Voltage and Current Generation in Carbon Nanotubes. *Phys. Rev. B: Condens. Matter Mater. Phys.* **2004**, *70*, 205423.
- (11) Ghosh, S.; Sood, A. K.; Kumar, N. Carbon Nanotube Flow Sensors. *Science* **2003**, *299*, 1042.
- (12) Liu, J.; Dai, L.; Baur, J. W. Multiwalled Carbon Nanotubes for Flow-Induced Voltage Generation. *J. Appl. Phys.* **2007**, *101*, 064312.
- (13) Zhao, Y.; Song, L.; Deng, K.; Liu, Z.; Zhang, Z.; Yang, Y.; Wang, C.; Yang, H.; Jin, A.; Luo, Q.; et al. Individual Water-Filled Single-Walled Carbon Nanotubes as Hydroelectric Power Converters. *Adv. Mater.* **2008**, *20*, 1772–1776.
- (14) Yuan, Q.; Zhao, Y.-P. Hydroelectric Voltage Generation Based on Water-Filled Single-Walled Carbon Nanotubes. *J. Am. Chem. Soc.* **2009**, *131*, 6374–6376.
- (15) Liu, Z.; Zheng, K.; Hu, L.; Liu, J.; Qiu, C.; Zhou, H.; Huang, H.; Yang, H.; Li, M.; Gu, C.; et al. Surface-Energy Generator of Single-Walled Carbon Nanotubes and Usage in a Self-Powered System. *Adv. Mater.* **2010**, *22*, 999–1003.
- (16) Xu, B.; Chen, X. Liquid Flow-Induced Energy Harvesting in Carbon Nanotubes: A Molecular Dynamics Study. *Phys. Chem. Chem. Phys.* **2013**, *15*, 1164–1168.
- (17) Kim, J.; Lee, J.; Kim, S.; Jung, W. Highly Increased Flow-Induced Power Generation on Plasmonically Carbonized Single-Walled Carbon Nanotube. *ACS Appl. Mater. Interfaces* **2016**, *8*, 29877–29882.
- (18) Ho Lee, S.; Kim, D.; Kim, S.; Han, C.-S. Flow-Induced Voltage Generation in High-Purity Metallic and Semiconducting Carbon Nanotubes. *Appl. Phys. Lett.* **2011**, *99*, 104103.
- (19) Liew, K. M.; Wong, C. H.; He, X. Q.; Tan, M. J.; Meguid, S. A. Nanomechanics of Single and Multiwalled Carbon Nanotubes. *Phys. Rev. B: Condens. Matter Mater. Phys.* **2004**, *69*, 115429.
- (20) Yin, J.; Zhang, Z.; Li, X.; Zhou, J.; Guo, W. Harvesting Energy from Water Flow over Graphene? *Nano Lett.* **2012**, *12*, 1736–1741.
- (21) Guan, Y.; Shao, Q.; Chen, W.; Liu, S.; Zhang, X.; Deng, Y. Dynamic Three-Dimensional Nanowetting Behavior of Imidazolium-Based Ionic Liquids Probed by Molecular Dynamics Simulation. *J. Phys. Chem. C* **2017**, *121*, 23716–23726.
- (22) Zhang, S.; Zhang, J.; Zhang, Y.; Deng, Y. Nanoconfined Ionic Liquids. *Chem. Rev.* **2017**, *117*, 6755–6833.
- (23) Zhang, S.; Zhang, Q.; Zhang, Y.; Chen, Z.; Watanabe, M.; Deng, Y. Beyond Solvents and Electrolytes: Ionic Liquids-Based Advanced Functional Materials. *Prog. Mater. Sci.* **2016**, *77*, 80–124.
- (24) Ghoufi, A.; Szymczyk, A.; Malfreyt, P. Ultrafast Diffusion of Ionic Liquids Confined in Carbon Nanotubes. *Sci. Rep.* **2016**, *6*, 28518.
- (25) Martínez, L.; Andrade, R.; Birgin, E. G.; Martínez, J. M. Packmol: A Package for Building Initial Configurations for Molecular Dynamics Simulations. *J. Comput. Chem.* **2009**, *30*, 2157–2164.
- (26) Todorov, I. T.; Smith, W.; Trachenko, K.; Dove, M. T. DL_Poly_3: New Dimensions in Molecular Dynamics Simulations Via Massive Parallelism. *J. Mater. Chem.* **2006**, *16*, 1911–1918.
- (27) Liu, Z.; Huang, S.; Wang, W. A Refined Force Field for Molecular Simulation of Imidazolium-Based Ionic Liquids. *J. Phys. Chem. B* **2004**, *108*, 12978–12989.
- (28) Allen, M. P.; Tildesley, D. J. *Computer Simulation of Liquids*; Oxford University Press, 2017.
- (29) Hoover, W. G. Canonical Dynamics: Equilibrium Phase-Space Distributions. *Phys. Rev. A: At., Mol., Opt. Phys.* **1985**, *31*, 1695–1697.
- (30) Nosé, S. A Unified Formulation of the Constant Temperature Molecular Dynamics Methods. *J. Chem. Phys.* **1984**, *81*, 511–519.
- (31) Essmann, U.; Perera, L.; Berkowitz, M. L.; Darden, T.; Lee, H.; Pedersen, L. G. A Smooth Particle Mesh Ewald Method. *J. Chem. Phys.* **1995**, *103*, 8577–8593.
- (32) Yong, W. C.; Todorov, T. I. DL_Analyser Notation for Atomic Interactions (Danai): A Natural Annotation System for Molecular Interactions, Using Ethanoic Acid Liquid as a Test Case. *Molecules* **2018**, *23*, 36.
- (33) Humphrey, W.; Dalke, A.; Schulten, K. VMD: Visual Molecular Dynamics. *J. Mol. Graphics* **1996**, *14*, 33–38.
- (34) de Pablo, P. J.; Gómez-Navarro, C.; Colchero, J.; Serena, P. A.; Gómez-Herrero, J.; Baró, A. M. Nonlinear Resistance Versus Length in Single-Walled Carbon Nanotubes. *Phys. Rev. Lett.* **2002**, *88*, 036804.
- (35) Shao, Q.; Jia, J.; Guan, Y.; He, X.; Zhang, X. Flow-Induced Voltage Generation by Moving a Nano-Sized Ionic Liquids Droplet over a Graphene Sheet: Molecular Dynamics Simulation. *J. Chem. Phys.* **2016**, *144*, 124703.
- (36) Afandak, A.; Eslami, H. Ion-Pairing and Electrical Conductivity in the Ionic Liquid 1-N-Butyl-3-Methylimidazolium Methylsulfate [Bmim][MeSO₄]: Molecular Dynamics Simulation Study. *J. Phys. Chem. B* **2017**, *121*, 7699–7708.
- (37) Guan, Y.; Shao, Q.; Chen, W.; Zhang, J.; Zhang, X.; Deng, Y. Flow-Induced Voltage Generation by Driving Imidazolium-Based Ionic Liquids over a Graphene Nano-Channel. *J. Mater. Chem. A* **2018**, *6*, 11941–11950.
- (38) Rajput, N. N.; Monk, J.; Singh, R.; Hung, F. R. On the Influence of Pore Size and Pore Loading on Structural and Dynamical Heterogeneities of an Ionic Liquid Confined in a Slit Nanopore. *J. Phys. Chem. C* **2012**, *116*, 5169–5181.
- (39) Sun, L.; Morales-Collazo, O.; Xia, H.; Brennecke, J. F. Effect of Structure on Transport Properties (Viscosity, Ionic Conductivity, and Self-Diffusion Coefficient) of Aprotic Heterocyclic Anion (Aha) Room-Temperature Ionic Liquids. 1. Variation of Anionic Species. *J. Phys. Chem. B* **2015**, *119*, 15030–15039.
- (40) Tsuzuki, S.; Shinoda, W.; Saito, H.; Mikami, M.; Tokuda, H.; Watanabe, M. Molecular Dynamics Simulations of Ionic Liquids: Cation and Anion Dependence of Self-Diffusion Coefficients of Ions. *J. Phys. Chem. B* **2009**, *113*, 10641–10649.
- (41) Tokuda, H.; Hayamizu, K.; Ishii, K.; Susan, M. A. B. H.; Watanabe, M. Physicochemical Properties and Structures of Room Temperature Ionic Liquids. 1. Variation of Anionic Species. *J. Phys. Chem. B* **2004**, *108*, 16593–16600.
- (42) Ohba, T. The Thinnest Molecular Separation Sheet by Graphene Gates of Single-Walled Carbon Nanohorns. *ACS Nano* **2014**, *8*, 11313–11319.